Catalytic Hydrolysis of Ammonia Borane *via* Cobalt Palladium Nanoparticles

Daohua Sun,[†,‡,*] Vismadeb Mazumder,[†] Önder Metin,[†,§] and Shouheng Sun[†,*]

[†]Department of Chemistry, Brown University, Providence, Rhode Island 02912, United States, [‡]Department of Chemical and Biochemical Engineering, College of Chemistry and Chemical Engineering, Xiamen University, Xiamen 361005, China, and [§]Department of Chemistry, Faculty of Science, Atatürk University, 25240 Erzurum, Turkey

ABSTRACT Monodisperse 8 nm CoPd nanoparticles (NPs) with controlled compositions were synthesized by the reduction of cobalt acetylacetonate and palladium bromide in the presence of oleylamine and trioctylphosphine. These NPs were active catalysts for hydrogen generation from the hydrolysis of ammonia borane (AB), and their activities were composition dependent. Among the 8 nm CoPd catalysts tested for the hydrolysis of AB, the $Co_{35}Pd_{65}$ NPs exhibited the highest catalytic activity and durability. Their hydrolysis completion time and activation energy were 5.5 min and 27.5 kJ mol^{-1}, respectively, which were comparable to the best Pt-based catalyst reported. The catalytic performance of the CoPd/C could be further enhanced by a preannealing treatment at 300 °C under air for 15 h with the hydrolysis completion time reduced to 3.5 min. This high catalytic performance of $Co_{35}Pd_{65}$ NP catalyst makes it an exciting alternative in pursuit of practical implementation of AB as a hydrogen storage material for fuel cell applications.

KEYWORDS: ammonia borane hydrolysis · bimetallic nanoparticles · cobalt–palladium alloy catalyst · heterogeneous catalysis · hydrogen storage

Ammonia borane (AB) complex $H_3N{\cdot}BH_3$ is considered to be the most promising candidate for "on-board" hydrogen applications among all other practical hydrogen storage materials.[1,2] It has a high hydrogen content (19.6% wt) and is soluble/stable in aqueous solutions. More importantly, it is able to release hydrogen *via* a room-temperature hydrolysis reaction in the presence of a suitable catalyst.[3−10] In its complete hydrolysis reaction, one mole of AB complex can generate three moles of hydrogen (H_2):[11] $H_3N{\cdot}BH_3(aq) + 2\ H_2O \rightarrow NH_4BO_2(aq) + 3\ H_2(g)$.

The catalysts tested for AB hydrolysis have mainly included nanoparticles (NPs) of noble metals Rh, Ir, Ru, and Pt,[12−15] which are all unsuitable for practical applications due to their limited resources and high price tags. Recently, NP catalysts based on the first-row transition metals Fe,[16] Ni,[17−21] and Co[22−24] have also been studied, but they have only moderate catalytic activity and lack the needed stability in the hydrolysis conditions. To make the AB complex a practical H_2 reservoir for "on board" applications, highly efficient catalysts with much reduced usage of noble metals Rh, Ir, Ru, and Pt or, ideally, with non-noble metals are desired. Recent research has indicated that bimetallic NPs containing an alloy structure of a noble metal and a first-row transition metal have composition-dependent optical, magnetic, and catalytic properties that are different from any of the monometallic NP components.[25] With proper control of size, morphology, and compositions, their physical and chemical properties can be greatly enhanced.[26−28] These binary alloy NPs may provide a solution for the future design and synthesis of practical catalysts for AB hydrolysis and H_2 generation.

Herein we report the synthesis of 8 nm monodisperse CoPd alloy NPs and study their catalytic hydrolysis of the AB complex in water at room temperature. We chose Co and Pd as the constituents of the bimetallic catalyst based on the fact that Co NPs have the highest activity among the non-noble metal catalysts[22−24] and Pd NPs are moderately active among the noble metal catalysts[13,29] for AB hydrolysis. We demonstrate that the activity and stability of these CoPd NPs can be improved by controlling their compositions. The optimum catalyst is $Co_{35}Pd_{65}$ NPs with their catalytic efficiency close to the benchmark Pt catalyst.

RESULTS AND DISCUSSION

Monodisperse 8 nm CoPd NPs were synthesized by the reduction of $Co(acac)_2$ (acac = acetylacetonate) and $PdBr_2$ in the presence of oleylamine (OAm) and trioctylphosphine (TOP) *via* a high-temperature solution phase synthesis procedure. In this synthesis, OAm acted as the solvent, surfactant, and reductant, and TOP served as a

* Address correspondence to sdaohua@xmu.edu.cn; ssun@brown.edu.

Received for review May 6, 2011 and accepted July 18, 2011.

Published online July 18, 2011
10.1021/nn2016666

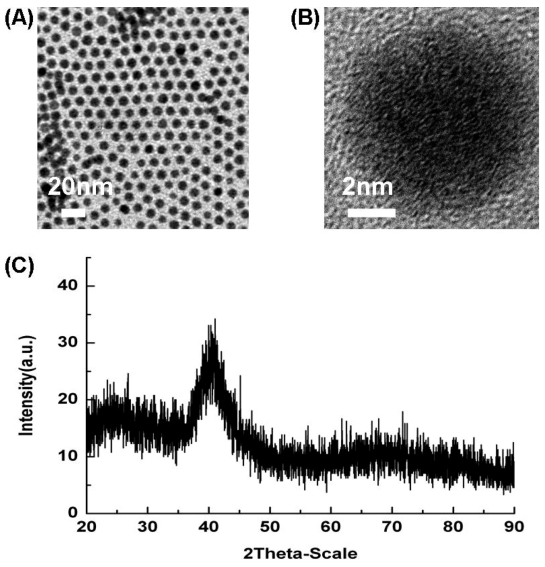

Figure 1. (A) TEM and (B) HRTEM image of the 8 nm $Co_{35}Pd_{65}$ NPs and (C) XRD pattern of the 8 nm $Co_{35}Pd_{65}$ NPs.

co-surfactant. Different from what we have reported in the synthesis of Pd NPs,[29] both $PdBr_2$ and TOP seemed to be the key for the formation of the CoPd alloy structure. Without them, the NP quality was very poor and the NP product was often contaminated with elemental Co and Pd NPs. The detailed synthesis of CoPd and other Pd-based binary alloy NPs will be published elsewhere. Figure 1A shows a transmission electron microscopy (TEM) image of the 8 nm CoPd NPs obtained from the synthesis for the current catalytic studies. The NPs have a narrow size distribution with a standard deviation of 9% with respect to NP diameter. High-resolution TEM (HRTEM) studies of a series of single CoPd NPs show that the as-synthesized CoPd NPs have a polycrystalline structure (Figure 1B). This polycrystalline nature is further confirmed by the X-ray diffraction pattern of the NPs (Figure 1C).

Both metal content and Co/Pd composition of the OAm- and TOP-coated CoPd NPs were analyzed by inductively coupled plasma atomic emission spectroscopy (ICP-AES). The 8 nm CoPd NPs generally contain 30 wt % of Co/Pd metals. The Co/Pd composition of the CoPd NPs was controlled by the initial molar ratio of the Co and Pd salts. Using metal salts with the Co/Pd ratio of 4:1, 3:2, 1:1, 2:3, and 1:4, we obtained $Co_{79}Pd_{21}$, $Co_{35}Pd_{65}$, $Co_{27}Pd_{73}$, $Co_{14}Pd_{86}$, and Co_5Pd_{95} NPs, respectively. Figure S1 also displays more representative TEM images of the CoPd NPs used for catalytic studies. The NPs are all 7−10 nm with narrow size distribution, making it possible to compare their composition-dependent activities and to choose optimum composition for detailed analyses in AB hydrolysis kinetics. We also made 4.5 nm Pd NPs[29] and studied their AB hydrolysis to demonstrate that the hydrolysis activity of the CoPd NPs was enhanced by alloying Pd with Co.

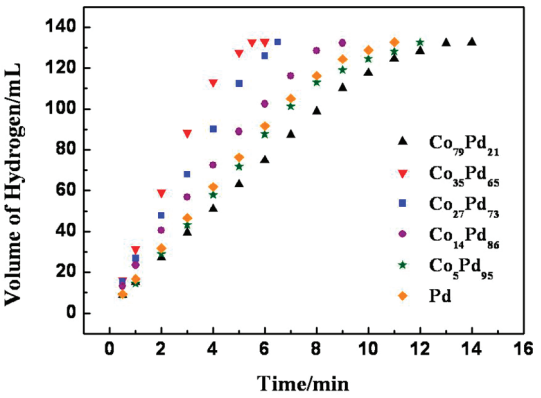

Figure 2. Plot of time *vs* volume of H_2 generated from AB hydrolysis catalyzed by CoPd/C with different CoPd compositions and Pd/C (CoPd NPs = 15 mg, Pd NPs = 15 mg, [AB] = 200 mM, $T = 25 \pm 1$ °C).

To study NP catalysis, the as-synthesized CoPd NPs (15 mg) were first deposited on Ketjen carbon support (45 mg) (25 wt % of NPs) and mixed with AB aqueous solution at room temperature under a fast magnetic stirring. H_2 generated from the AB hydrolysis was collected in the buret with which the H_2 volume was measured. Figure 2 is a plot of the H_2 gas generated *versus* time for every 10 mL of AB (2 mmol, 200 mM) solution in the presence of 15 mg of CoPd NPs. From these curves, we can see that when 2 mmol of AB complex is completely hydrolyzed, 6 mmol of H_2 (~134 mL) is generated. This corresponds to the full hydrolysis of AB complex with one mole of AB producing three moles of H_2. The sooner the hydrolysis is completed, the more active the NP catalyst is. From the plot, we can see that CoPd NPs with too much Co ($Co_{79}Pd_{21}$) or Pd (Co_5Pd_{95}) show even lower activity than the pure Pd NPs. $Co_{14}Pd_{86}$, $Co_{27}Pd_{73}$, and $Co_{35}Pd_{65}$ NPs have a higher activity than the Pd NPs. Under our evaluation conditions, the $Co_{35}Pd_{65}$ NPs/C catalyst is the most active in catalyzing the AB hydrolysis reaction with a completion time of 5.5 min. Here, better catalytic activity of $Co_{35}Pd_{65}$ than pure Pd NPs might be explained by the Sabatier principle, which states that optimal catalytic activity can be achieved on a catalytic surface with median binding energies of reactive intermediates.[30] If the reactant binds to the catalyst surface too weakly, then it cannot be activated. However, if it binds to the surface too strongly, it will occupy all available surface sites and poison the catalyst.[31] Thus, it appears that there is an optimal ratio between Pd and Co to show the highest catalytic activity for AB hydrolysis.

Since $Co_{35}Pd_{65}$ NPs have the highest hydrolysis activity among all the NPs prepared in this work, their AB hydrolysis kinetics is further evaluated. This was done by varying catalyst concentrations, substrate concentrations, and temperatures. In the NP concentration-dependent hydrolysis study, the hydrolysis reaction was carried out under different NP concentrations

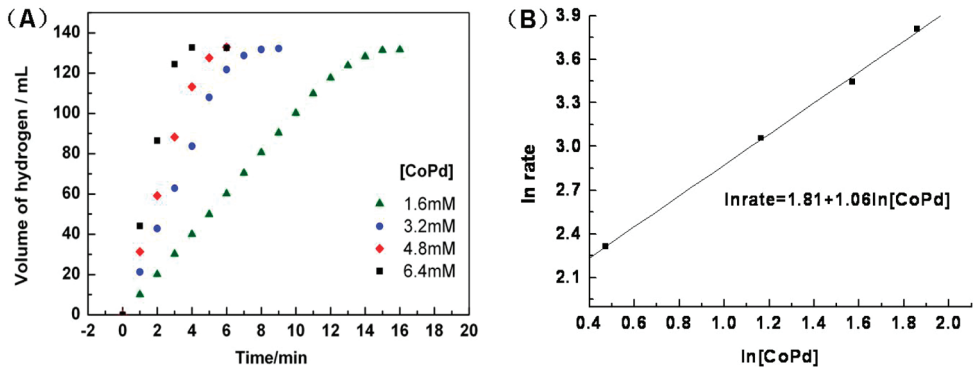

Figure 3. (A) Plot of time *vs* volume of hydrogen generated from hydrolysis of AB catalyzed by $Co_{35}Pd_{65}$/C catalyst at different catalyst concentrations ([AB] = 200 mM, $T = 25 \pm 1$ °C). (B) Plot of hydrogen generation rate *vs* catalyst concentration in logarithmic scale.

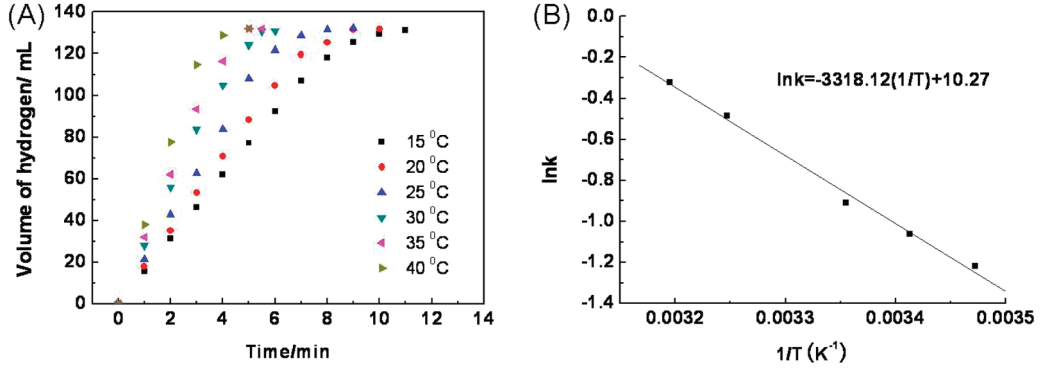

Figure 4. (A) Plot of time *vs* volume of hydrogen generated from hydrolysis of AB catalyzed by $Co_{35}Pd_{65}$/C catalyst at different temperatures ([AB] = 200 mM, [CoPd] = 3.2 mM). (B) Arrhenius plot of ln *k vs* (1/*T*).

of 1.6, 3.2, 4.8, and 6.4 mM (representing 5, 10, 15, and 20 mg of $Co_{35}Pd_{65}$ NPs, respectively), while the initial AB concentration was kept constant at 200 mM. In AB concentration-dependent hydrolysis, the NP concentration was kept at 4.8 mM, while the AB concentrations were set at 50, 100, 150, and 200 mM. Finally, to obtain the activation energy (E_a) of the hydrolysis reaction, AB (200 mM) was hydrolyzed in the presence of 3.2 mM CoPd NPs at various temperatures (15−40 °C). In all these tests, the gas reaction product was characterized by the acid−base titration method to ensure ammonia was not formed *via* a direct decomposition of AB or other reaction pathways. Our tests showed no sign of ammonia, indicating that the gas generated during the reaction was pure H_2.

Figure 3A shows the plots of time *versus* volume of H_2 generated from AB hydrolysis catalyzed by the $Co_{35}Pd_{65}$/C catalyst at different catalyst concentrations at temperature $T = 25 \pm 1$ °C. A rapid and almost linear H_2 gas evolution was observed. A stoichometric amount of H_2 (~6 mmol) was generated within less than 15 min. Figure 3B is the plot of H_2 generation rate *versus* CoPd concentration in the logarithmic scale. The slope of 1.06 indicates that the hydrolysis of AB catalyzed by the 8 nm $Co_{35}Pd_{65}$/C catalyst is first-order with respect to the catalyst concentration. The H_2 generation rate was found to be practically independent of AB concentration (shown in Figure S2A). Figure S2B shows the plot of H_2 generation rate *versus* AB concentration in logarithmic scale. The nearly horizontal line (slope of 0.05) indicates that the hydrolysis catalyzed by the 8 nm $Co_{35}Pd_{65}$/C catalyst is zero-order with respect to the concentration of AB. This infers that in the hydrolysis reaction the adsorption of AB on the catalyst surface is a rate-limiting step.

Figure 4 shows the plot of time *versus* volume of H_2 generated during AB hydrolysis at various temperatures. The values of the rate constant *k* at different temperatures were calculated from the slope of the linear part of each plot in Figure 4A for determining the activation energy. Figure 4B shows the Arrhenius plot (ln *k vs* 1/*T*), from which E_a for the hydrolysis is calculated to be 27.5 kJ mol^{-1}. Its activity can be further evaluated in terms of a total turnover frequency (TOF) value (mol of H_2·(mol of catalyst·min)$^{-1}$), which is 22.7. Compared with what has been reported on the performance of various Co-, Pd-, and Pt-based catalysts for the hydrolysis of AB at room temperature (Table 1), the $Co_{35}Pd_{65}$/C catalyst is among the most active. Its catalytic activity is even close to Pt-based Pt/C, PtO_2, and Pt black catalysts. We should note that in Table 1 (1) the completion time for Pt catalysts varies in a wide range due to the NP size and supporting materials effects and (2) the data obtained from Co NPs[23] cannot

TABLE 1. H_2 Generation from Aqueous AB Catalyzed by Co-, Pd-, and Pt-Based Catalysts

catalyst	metal/AB ratio (mol/mol)	maximum H_2/AB ratio (mol/mol)	completion time (min)	TOF (mol H_2 · mol catalyst^{-1} · min^{-1})	activation energy E_a (kJ · mol^{-1})	ref
40 wt % Pt/C	0.018	3.0	3	55.56	21−23	9
PtO_2	0.018	3.0	8	20.83		9
Pt black	0.018	3.0	12	13.89		9
K_2PtCl_4	0.018	3.0	19	8.77		9
2 wt % Pd/γ-Al_2O_3	0.018	3.0	120	1.39		9
Pd black	0.018	3.0	250	0.67		9
10 wt % Co/γ-Al_2O_3	0.018	2.9	70	2.30	62	9
10 wt % Co/SiO_2	0.018	2.9	70	2.30		9
10 wt % Co/C	0.018	2.9	55	2.92		9
Pd/zeolite	0.02	3.0	24	6.25	56	32
Co/zeolite	0.02	3.0	28	5.36	56	33
PVP-Co	0.025	3.0	25	4.80	46	22
PSSA-co-MA-Pd	0.05	3.0	12	5	44	13
Co	0.04	3.0	1.7	44.2		23
Au@Co	0.02	3.0	11	13.7		34
25 wt % $Co_{35}Pd_{65}$/C	0.024	3.0	5.5	22.7	27.5	this study
$Co_{35}Pd_{65}$/C annealed	0.024	3.0	3.5	35.7		this study

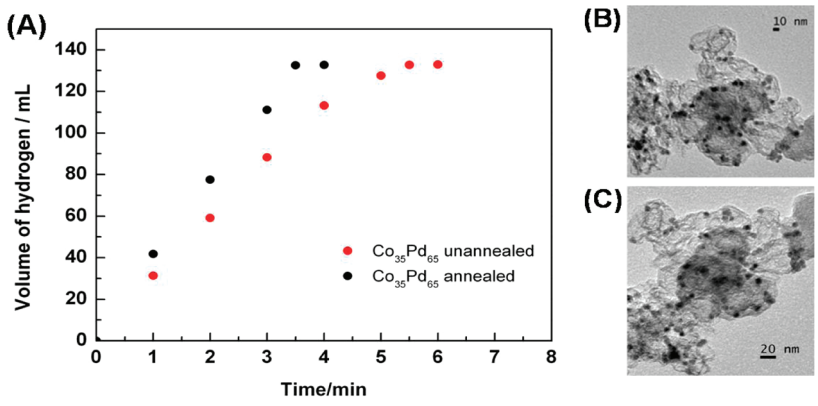

Figure 5. (A) Plot of time *vs* volume of H_2 generated from hydrolysis of AB catalyzed by $Co_{35}Pd_{65}$/C catalyst unannealed and annealed ([AB] = 200 mM, [CoPd] = 4.8 mM, $T = 25 \pm 1$ °C) and TEM images of $Co_{35}Pd_{65}$/C NPs before (B) and after (C) 300 °C annealing in air for 15 h.

prove that Co NPs are more active, as the measured volume of hydrogen is likely from both AB and $NaBH_4$, a reducing agent used in the synthesis of Co NPs in H_3NBH_3.

The catalytic performance of the as-prepared CoPd/C can be further enhanced by a preannealing treatment. In this study, we first annealed the $Co_{35}Pd_{65}$/C catalyst at 300 °C under air for 15 h. Figure S3 is the XRD pattern of the annealed $Co_{35}Pd_{65}$/C catalyst. Comparing with that in Figure 1C, we can see that the treatment did not oxidize the CoPd NPs; rather, the annealing led to the formation of better crystallinity in the alloy NPs. We then studied the AB hydrolysis catalyzed by this $Co_{35}Pd_{65}$/C catalyst. Figure 5A gives the volume of hydrogen generated from AB hydrolysis *versus* the reaction time. It shows that after annealing, the catalyst is more active with the hydrolysis completion time reduced to 3.5 min. The TOF value of the catalyst is also increased from 22.7 to 35.7. Since the $Co_{35}Pd_{65}$/C NPs have no morphology change after this thermal treatment (Figure 5B, C), the enhanced activity is due most likely to the more efficient surfactant removal and better alloy structure formation under the annealing conditions, which allows Co and Pd to function more synergetically for AB hydrolysis at room temperature.

The reusability of the as-synthesized $Co_{35}Pd_{65}$/C catalyst under the current room-temperature hydrolysis conditions was also tested. After every 24 h when H_2 generation was complete, another equivalent (2 mmol) of AB was added to the reaction system and the released gas was once again measured. As shown in Figure 6A, the catalyst shows no activity change in the first 72 h (the first three sets of data overlap with each other). After 120 h, the reaction completion time is increased to 7 min. The TEM image (shown in

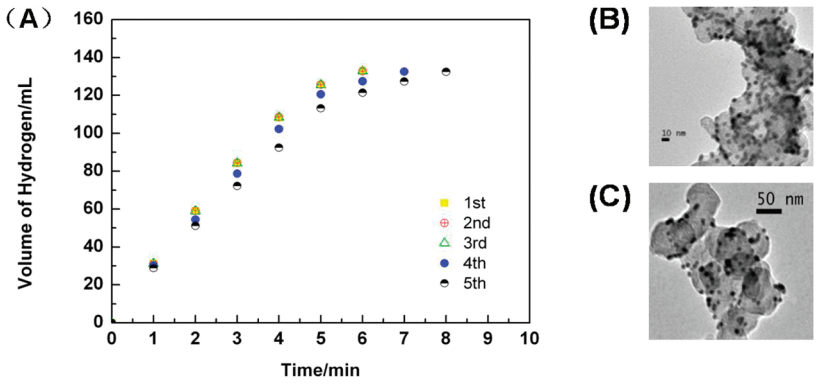

Figure 6. (A) Time *vs* volume of hydrogen generated from hydrolysis of AB catalyzed by $Co_{35}Pd_{65}$/C catalyst during a five-cycle reusability test ([CoPd] = 3.2 mM, [AB] = 200 mM, $T = 25 \pm 1$ °C); TEM images before (B) and after (C) five catalytic cycles.

Figure 6B,C) proves that there is no significant change in NP size or morphology during the test. Therefore, the slight activity drop is caused by the increase in concentration of metaborate and the viscosity of the solution during the AB hydrolysis. The lifetime of the catalyst in the AB hydrolysis was determined by measuring the volume of H_2 and calculating the total turnover number (TTON, moles of H_2/moles of catalyst). Figure S4 shows the variation in TTON and the volume of H_2 *versus* time plot during the hydrolysis of AB, from which we can see that the 8 nm $Co_{35}Pd_{65}$/C catalyst has 6675 turnovers over 45 h in the hydrolysis reaction at 25.0 °C before it is deactivated. Our experimental results suggest that the 8 nm $Co_{35}Pd_{65}$/C NPs are robust for AB hydrolysis. Once metaborate generated during the reaction is removed from the solution, the NPs should exhibit much higher activity and stability. They are a promising class of non-Pt catalyst for practical hydrolysis of AB and H_2 generation.

In summary, we have reported a unique solution phase synthesis of monodisperse 8 nm CoPd NPs with controlled compositions and studied their catalytic hydrolysis of ammonia borane in aqueous solutions. The CoPd NPs show the composition-dependent activity for AB hydrolysis at room temperature, with $Co_{35}Pd_{65}$ NPs being the most active. The kinetic studies on these $Co_{35}Pd_{65}$ NPs reveal that the catalytic hydrolysis of AB is first-order with respect to the catalyst concentration and zero-order with respect to substrate concentration. The activation energy for the hydrolysis reaction is 27.5 kJ mol^{-1}. The NP catalyst provides 6675 turnovers and shows the desired durability under the current hydrolysis conditions. The catalytic activity of these $Co_{35}Pd_{65}$/C NPs can be further enhanced by thermal annealing at 300 °C in air. The reported synthesis may represent a new approach to non-Pt catalysts for future development of ammonia borane into a practical hydrogen storage material for renewable energy applications.

MATERIALS AND METHODS

Chemicals. Chemicals for the NP synthesis and ammonia borane complex (97%) were purchased from Sigma Aldrich and used as received. Deionized water was used for all hydrolysis experiments.

Synthesis of Monodisperse CoPd NPs. Under a gentle nitrogen flow, 0.3 mmol of $Co(acac)_2$ (acac = acetylacetonate), 0.2 mmol of $PdBr_2$, and 1 mL of TOP were mixed with 18 mL of OAm. The mixture was heated to 260 °C at a heating rate of 5 °C min^{-1}. The solution was kept at 260 °C for an hour before it was cooled to room temperature. Then 40 mL of 2-propanol was added and the product was separated by centrifugation at 8000 rpm for 8 min. The product was then dispersed in hexane. ICP analysis revealed the composition of the as-synthesized NPs to be $Co_{35}Pd_{65}$. The alloy composition could be controlled by the ratio of $Co(acac)_2$ to $PdBr_2$.

Synthesis of CoPd/C Catalyst. A 15 mg amount of 8 nm CoPd NPs was dissolved in 5.0 mL of hexane and 5.0 mL of acetone in a 20.0 mL glass vial and mixed with 45 mg of Ketjen carbon (surface area 800 m^2/g) support. The mixture was sonificated for 30 min to ensure complete absorption of NPs onto the carbon support. After evaporation of hexane/acetone under a gentle nitrogen flow, the solid residue was suspended in 10.0 mL of deionized water by sonication for 30 min.

Hydrolysis of AB Catalyzed by CoPd/C Catalysts. The catalytic activity of the 8 nm CoPd NPs/C catalysts toward hydrolysis of AB was determined by measuring the rate of hydrogen generation in a typical water-filled gas buret system. Before starting the catalytic activity test, a jacketed reaction flask (25 mL) containing a Teflon-coated stir bar was placed on a magnetic stirrer and thermostated to 25.0 ± 1 °C by circulating water through its jacket from a constant-temperature bath. Then, a buret filled with water was connected to the reaction flask to measure the volume of hydrogen gas evolved from the reaction. Next, a 10.0 mL aqueous suspension of the catalyst was transferred into the reaction flask, and 64.0 mg (2 mmol) of AB was added into the catalyst solution at 800 rpm stirring rate. The volume of hydrogen gas evolved was measured by recording the displacement of water level every minute. The reaction was considered to cease when no hydrogen gas generation was observed. For a control experiment, 64 mg of AB and 45 mg of Ketjen carbon were dissolved in 20.0 mL of H_2O without any catalytic materials present. No hydrogen generation was observed in 24 h. A ^{11}B NMR spectrum of the solution after one day showed only metaborate's signal at −23.9 ppm.

Catalyst Reusability in the Hydrolysis of AB. After the hydrogen generation reaction was completed, the as-synthesized CoPd/C catalysts were kept in the reaction solution under ambient conditions, and another equivalent of AB (64 mg, 2 mmol)

was added to the reaction system after 24 h. The gas generation was monitored by volume changes in the buret. The process was repeated in a 120 h period until catalyst activity started to drop.

Catalyst Lifetime in the Hydrolysis of AB. The lifetime of the 8 nm CoPd/C catalyst in the hydrolysis of AB was determined by measuring the total turnover number (moles of H_2/mols of catalyst). The experiment was performed in a 20.0 mL aqueous solution containing 15.0 mg of CoPd NPs on 45.0 mg of carbon support and 256.0 mg of AB complex at 25.0 ± 1 °C. Once AB was all hydrolyzed (by checking the stoichiometric H_2 gas evolution (3.0 mol H_2/mol AB), the completion time was recorded, a new batch of AB was added, and the reaction was monitored the same way.

Characterizations. Samples for TEM analysis were prepared by depositing a single drop of diluted NP dispersion in hexane on amorphous carbon coated copper grids. Images were obtained with a JEOL 2010 TEM (200 kV). XRD patterns of the samples were collected on a Bruker AXS D8-Advanced diffractometer with Cu Kα radiation (λ = 1.5418 Å). The ICP-MS measurements were carried out on a JY2000 Ultrace ICP atomic emission spectrometer equipped with a JY AS 421 auto sampler and 2400 g/mm holographic grating. ^{11}B NMR spectra were recorded on a JEOL JNM-AL400 spectrometer operating at 128.15 MHz.

Acknowledgment. The work was supported in part by ExxonMobil (S.S.), the National Natural Science Foundation of China No. 21036004 (D.S.), and the Scientific and Technological Research Council of Turkey (TUBITAK) for the 2214-Research fellowship program and the METU-DPT-OYP program on behalf of Ataturk University (Ö.M.).

Supporting Information Available: TEM images of the $Co_{79}Pd_{21}$, $Co_{27}Pd_{73}$, $Co_{14}Pd_{86}$, and Co_5Pd_{95} NPs; the plot of time *vs* volume of hydrogen generated from AB hydrolysis catalyzed by $Co_{35}Pd_{65}$/C catalyst at different AB concentrations; XRD pattern of $Co_{35}Pd_{65}$/C after annealing; total turnover number and volume of hydrogen *vs* time plot for $Co_{35}Pd_{65}$/C. This material is available free of charge *via* the Internet at http://pubs.acs.org.

REFERENCES AND NOTES

1. Schlapbach, L.; Züttel, A. Hydrogen Storage Materials for Mobile Applications. *Nature* **2001**, *414*, 353–358.
2. Grochala, W.; Edwards, P. P. Thermal Decomposition of the Noninterstitial Hydrides for the Storage and Production of Hydrogen. *Chem. Rev.* **2004**, *104*, 1283–1316.
3. Stephens, F. H.; Pons, V.; Baker, R. T. Ammonia-Borane: the Hydrogen Source par Excellence? *Dalton Trans.* **2007**, *25*, 2613–2626.
4. Mohajeri, N.; Raissi, A.; Adebiyi, O. Hydrolytic Cleavage of Ammonia-Borane Complex for Hydrogen Production. *J. Power Sources* **2007**, *167*, 482–485.
5. Umegaki, T.; Yan, J. M.; Zhang, X. B.; Shioyama, H.; Kuriyama, N.; Xu, Q. Boron- and Nitrogen-Based Chemical Hydrogen Storage Materials. *Int. J. Hydrogen Energy* **2008**, *34*, 2303–2311.
6. Hamilton, C. W.; Baker, R. T.; Staubitz, A.; Manners, I. B-N Compounds for Chemical Hydrogen Storage. *Chem. Soc. Rev.* **2009**, *38*, 279–293.
7. Jiang, H. L.; Singh, S. K.; Yan, J. M.; Zhang, X. B.; Xu, Q. Liquid Phase Chemical Hydrogen Storage: Catalytic Hydrogen Generation under Ambient Conditions. *Chem. Sus. Chem.* **2010**, *3*, 541–549.
8. Chandra, M.; Xu, Q. Dissociation and Hydrolysis of Ammonia Borane with Solid Acids and Carbon Dioxide: an Efficient Hydrogen Generation System. *J. Power Sources* **2006**, *159*, 855–860.
9. Xu, Q.; Chandra, M. A Portable Hydrogen Generation System: Catalytic Hydrolysis of Ammonia-Borane. *J. Alloys Compd.* **2007**, *446–447*, 729–732.
10. Ramachandran, P. V.; Gagare, P. D. Preparation of Ammonia Borane in High Yield and Purity, Methanolysis and Regeneration. *Inorg. Chem.* **2007**, *46*, 7810–7817.
11. Chandra, M.; Xu, Q. A High-Performance Hydrogen Generation System: Transition Metal-Catalyzed Dissociation and Hydrolysis of Ammonia–Borane. *J. Power Sources* **2006**, *156*, 190–194.
12. Clark, T. J.; Whittell, G. R.; Manners, I. Highly Efficient Colloidal Cobalt- and Rhodium-Catalyzed Hydrolysis of H_3NBH_3 in Air. *Inorg. Chem.* **2007**, *46*, 7522–7527.
13. Metin, Ö.; Sahin, S.; Özkar, S. Water-Soluble Poly (4-Styrenesulfonic Acid-co-Maleic Acid) Stabilized Ruthenium(0) and Palladium(0) Nanoclusters as Highly Active Catalysts in Hydrogen Generation from the Hydrolysis of Ammonia-Borane. *Int. J. Hydrogen Energy* **2009**, *34*, 6304–6313.
14. Chandra, M.; Xu, Q. Room Temperature Hydrogen Generation from Aqueous Ammonia-Borane Using Noble Metal Nanoclusters as Highly Active Catalysts. *J. Power Sources* **2007**, *168*, 135–142.
15. Basu, S.; Brockman, A.; Gagare, P.; Zheng, Y.; Ramachandran, P. V.; Delgass, W. N. Chemical Kinetics of Ru-Catalyzed Ammonia Borane Hydrolysis. *J. Power Sources* **2009**, *188*, 238–243.
16. Yan, J. M.; Zhang, X. B.; Han, S.; Shioyama, H.; Xu, Q. Iron Nanoparticle-Catalyzed Hydrolytic Dehydrogenation of Ammonia Borane for Chemical Hydrogen Storage. *Angew. Chem., Int. Ed.* **2008**, *47*, 2287–2289.
17. Umegaki, T.; Yan, J. M.; Zhang, X. B.; Shioyama, H.; Kuriyama, N.; Xu, Q. Preparation and Catalysis of Poly(N-Vinyl-2-Pyrrolidone) (PVP) Stabilized Nickel Catalyst for Hydrolytic Dehydrogenation of Ammonia Borane. *Int. J. Hydrogen Energy* **2009**, *34*, 3816–3822.
18. Yan, J. M.; Zhang, X. B.; Han, S.; Shioyama, H.; Xu, Q. Synthesis of Longtime Water/Air-Stable Ni Nanoparticles and Their High Catalytic Activity for Hydrolysis of Ammonia-Borane for Hydrogen Generation. *Inorg. Chem.* **2009**, *48*, 7389–7393.
19. Metin, Ö.; Mazumder, V.; Özkar, S.; Sun, S. H. Monodisperse Nickel Nanoparticles and Their Catalysis in Hydrolytic Dehydrogenation of Ammonia Borane. *J. Am. Chem. Soc.* **2010**, *132*, 1468–1469.
20. Metin, Ö; Özkar, S.; Sun, S. H. Monodisperse Nickel Nanoparticles Supported on SiO_2 as an Effective Catalyst for the Hydrolysis of Ammonia–Borane. *Nano. Res.* **2010**, *3*, 676–684.
21. Umegaki, T.; Yan, J. M.; Zhang, X. B.; Shioyama, H.; Kuriyama, N.; Xu, Q. Hollow Ni-SiO_2 Nanosphere-Catalyzed Hydrolytic Dehydrogenation of Ammonia Borane for Chemical Hydrogen Storage. *J. Power Sources* **2009**, *191*, 209–16.
22. Metin, Ö.; Özkar, S. Hydrogen Generation from the Hydrolysis of Ammonia-Borane and Sodium Borohydride Using Water Soluble Polymer-Stabilized Cobalt(0) Nanoclusters Catalyst. *Energy Fuels* **2009**, *23*, 3517–3526.
23. Yan, J. M.; Zhang, X. B.; Shioyama, H.; Xu, Q. Room Temperature Hydrolytic Dehydrogenation of Ammonia Borane Catalyzed by Co Nanoparticles. *J. Power Sources* **2010**, *195*, 1091–1094.
24. Metin, Ö.; Özkar, S. Water-Soluble Nickel(0) and Cobalt(0) Nanoclusters Stabilized by Poly (4-Styrenesulfonic Acid-co-Maleic Acid): Highly Active, Durable and Cost Effective Catalysts in Hydrogen Generation from the Hydrolysis of Ammonia-Borane. *Int. J. Hydrogen Energy* **2011**, *36*, 1424–1432.
25. Burda, C.; Chen, X. B.; Narayanan, R.; El-Sayed, M. A. Chemistry and Properties of Nanocrystals of Different Shapes. *Chem. Rev.* **2005**, *105*, 1025–1102.
26. Yao, C. F.; Zhuang, L.; Cao, Y. L.; Hi, X. P.; Yang, H. X. Hydrogen Release from Hydrolysis of Borazane on Pt- and Ni-Based Alloy Catalysts. *Int. J. Hydrogen Energy* **2008**, *33*, 2462–2467.
27. Yang, X. J.; Cheng, F. Y.; Liang, J.; Tao, Z. L.; Chen, J. Pt_xNi_{1-x} Nanoparticles as Catalysts for Hydrogen Generation from Hydrolysis of Ammonia Borane. *Int. J. Hydrogen Energy* **2009**, *34*, 8785–8791.
28. Yan, J. M.; Zhang, X. B.; Han, S.; Shioyama, H.; Xu, Q. Magnetically Recyclable Fe-Ni Alloy Catalyzed Dehydrogenation of Ammonia Borane in Aqueous Solution under Ambient Atmosphere. *J Power Sources* **2009**, *194*, 478–481.

29. Mazumder, V.; Sun, S. H. Oleylamine-Mediated Synthesis of Pd Nanoparticles for Catalytic Formic Acid Oxidation. *J. Am. Chem. Soc.* **2009**, *131*, 4588–4589.
30. Demirci, U. B.; Garin, F. Ru-Based Bimetallic Alloys for Hydrogen Generation by Hydrolysis of Sodium Tetrahydroborate. *J. Alloys Compd.* **2008**, *463*, 107–111.
31. Greeley, J.; Jaramillo, T. F.; Bonde, J.; Chorkendorff, I.; Nørskov, J. K. Computational High-Throughput Screening of Electrocatalytic Materials for Hydrogen Evolution. *Nat. Mater.* **2006**, *5*, 909–913.
32. Rakap, M.; Özkar, S. Zeolite Confined Palladium (0) Nanoclusters as Effective and Reusable Catalysts for Hydrogen Generation from the Hydrolysis of Ammonia-Borane. *Int. J. Hydrogen Energy* **2010**, *35*, 1305–1312.
33. Rakap, M.; Özkar, S. Hydrogen Generation from the Hydrolysis of Ammonia-Borane Using Intrazeolite Cobalt(0) Nanoclusters Catalyst. *Int. J. Hydrogen Energy* **2010**, *35*, 3341–3346.
34. Yan, J.-M.; Zhang, X.-B.; Akita, T.; Haruta, M.; Xu, Q. One-Step Seeding Growth of Magnetically Recyclable Au@Co Core−Shell Nanoparticles: Highly Efficient Catalyst for Hydrolytic Dehydrogenation of Ammonia Borane. *J. Am. Chem. Soc.* **2010**, *132*, 5326–5327.